

Effect of Temperature on Corrosion Behavior of VM110SS Casing Steel in the CO₂/H₂S Coexistent Environment

Naiyan Zhang¹, Dezhi Zeng^{1,*}, Zhiming Yu¹, Wentao Zhao², Junying Hu¹, Wenliang Deng³, Gang Tian⁴

¹ State Key Laboratory of Oil & Gas Reservoir Geology and Exploitation, Southwest Petroleum University, Chengdu 610500, China;

² PetroChina Southwest Oil and Gas Field Company, Luzhou 646000, China

³ China Petroleum Pipeline Engineering Co., Ltd, Langfang 065000, China

*E-mail: swpuzny@163.com

Received: 14 December 2017 / Accepted: 28 February 2018 / Published: 10 April 2018

The effect of temperature on the corrosion behavior of VM110SS casing steel in a H₂S/CO₂ co-existing environment was investigated by high temperature and high pressure (HTHP) autoclave and the electrochemical corrosion method. In addition, scanning electron microscopy (SEM) and energy dispersive spectrometry (EDS) were used to characterize the morphologies and structure of the corrosion scales. The results show that the corrosion rates of VM110SS steel in the gas-liquid two phase acidic environment exponentially increase in the initial stage and then decrease with the rise in temperature, and the corrosion rate reaches the peak at 90°C. The principal components of the product may be Fe_xS_y, indicating that the corrosion process is mainly dominated by H₂S. The corrosion scales with a porous flocculent structure can be detected in the gas phase; however, the corrosion scale with a brittle characteristic can be easily exfoliated in the liquid phase. Electrochemical tests show that the corrosion current density of VM110SS steel increases with the increase of temperature, and the total impedance decreases. The cathode process is greatly affected by temperature, and the corrosion reaction is mainly controlled by diffusion and activation. The investigation provides a theoretical basis for corrosion failure analysis of casing and technical guidance for material selection.

Keywords: H₂S/CO₂; VM110SS steel; temperature; corrosion scales; electrochemistry

1. INTRODUCTION

Over the last few years, the production of sour oil and gas has increased, especially in oil and gas fields in southwestern China [1-2]. As new areas are being explored, the exploitation of sour oil and gas fields has pushed the operation activities into more aggressive environments. Consequently, the service reliability of tubing and casing is the key to ensuring the safety development of oil and gas

fields. It has been reported that the failures of tubing and packer frequently occur [3-5], and these sour gases may easily escape and leak into the annular space between the tubing and casing (Figure 1). Carbon steel is widely used as a premium casing material due to its strength for withstanding the operation pressure and for its economic advantages [6-7]. However, carbon steel casings are exposed to sour media containing corrosive gases all year round, which poses a great threat to the casing integrity.

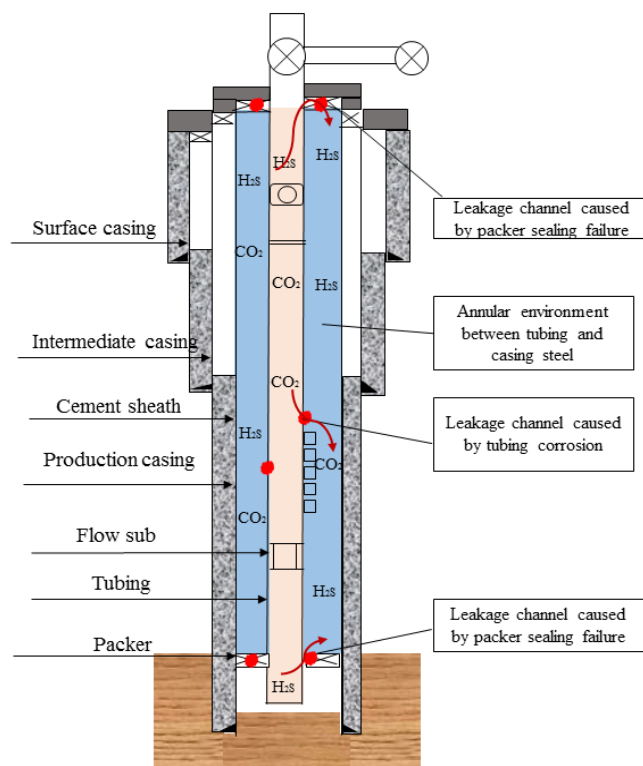


Figure 1. Schematic diagram of sour gases leakage

It has been widely acknowledged that temperature is one of the predominant factors affecting steel corrosion behavior [8-13]. As the temperature increases, the solubility of sour gases in the aqueous solution decreases, thereby alleviating the casing corrosion. This finding has been supported by many scholars. Afsharpour [8] illustrated that an increase in temperature led to lower solubility of acid gases (H_2S/CO_2). To verify this, Messabeh [9] experimentally measured CO_2 solubility in aqueous $CaCl_2$ solution at elevated temperatures using conductometric titration. In addition, the thermodynamics and kinetics of the casing corrosion process were changed and accelerated with the increase of temperature, thus promoting the corrosion development. Rauscher [10] found that the slopes of the cathodic Tafel lines anomalously changed with temperature. Robin [11] discovered that the corrosion current densities increased with the increase of temperature. Furthermore, the corrosion scale is greatly affected by temperature, especially corrosion scale formation/dissolution, structure, thickness, compactness, composition and stability [12-20]. Moreover, the critical temperature at the maximum corrosion rate varies with steel type and corrosion environment. Yin investigated the

corrosion behavior of SM 80SS tube steel in a stimulant solution containing H₂S and CO₂ and found that the maximum corrosion rate of the specimens occurred at 100°C [21].

To better understand the steel corrosion mechanism in a sour system at elevated temperature, this experimental study was undertaken to investigate the effect of temperature on VM110SS casing steel corrosion behavior in a H₂S/CO₂ gas field solution by means of weight-loss test, energy dispersive spectrometry (EDS), scanning electron microscopy (SEM) and electrochemical measurement. The investigation is valuable for safety assurance and materials selection of casing steel in high sulfur-containing gas fields.

2. EXPERIMENTAL

2.1 Material and specimen preparation

VM110SS casing steel, with a composition (mass fraction) of 0.25% C, 0.019% Si, 1.3% Mn, 0.009% P, 0.004% S, 0.16% Cr, 0.009% Ni and Fe balance, was employed in this test. According to the ASTM standards, the samples were processed into slices with dimensions of 30 mm×15 mm×3 mm and 10 mm×10 mm×5 mm for dynamic high temperature (HT) autoclave experiment and electrochemical measurement, respectively.

Prior to the experiment, in order to decrease the surface roughness, the samples were initially abraded by SiC paper progressively up to 1200 grit, then degreased with mineral ether and rinsed with anhydrous ethanol, and finally dried by air and stored in the desiccator for 4 h.

2.2 Weight-loss experiment

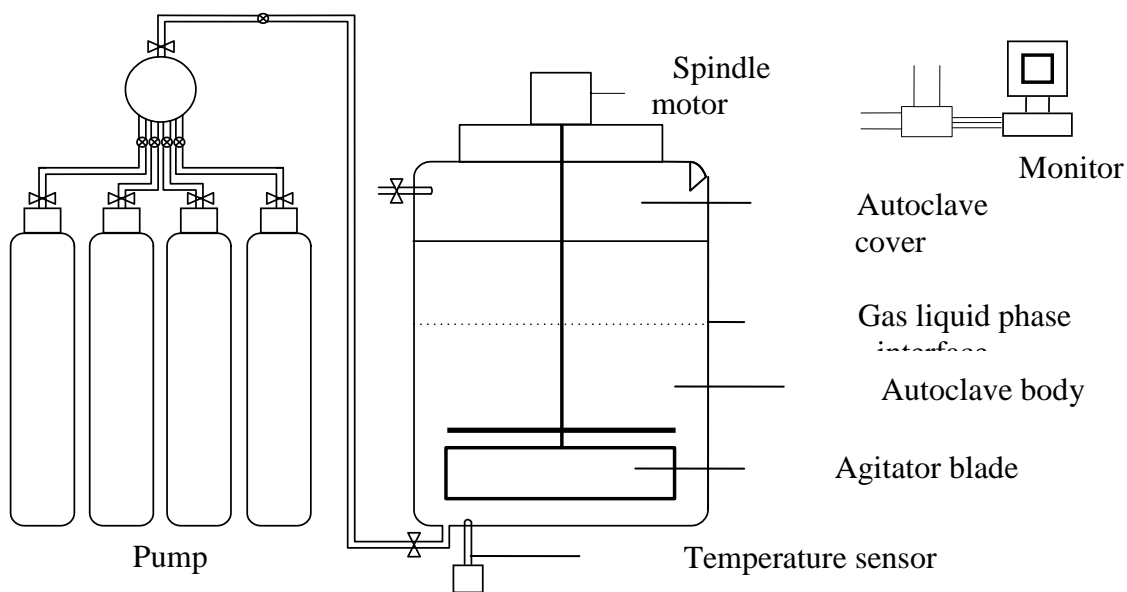


Figure 2. Schematic of the self – designed HT autoclave

The weight-loss tests were carried out in a self-designed high temperature (HT) autoclave, as shown in Figure 2. Before the test, all VM110SS samples were weighed using an electronic balance

(Model Sartorius BS110S) with a precision of 0.1 mg and then dried in air for 1 h before being exposed to the corrosive environment. The stimulated gas field produced water was deoxygenated by bubbling pure N₂ gas for 2 h. And its chemical composition is given in Table 1. For the immersion test, the stimulated gas field solution was poured into the HT autoclave. While heating to the required experimental temperature, the total pressure of corrosive gases was set as 18 Mpa with partial pressures of 0.4 Mpa H₂S and 0.55 Mpa CO₂ to start the experiment.

Table 1. Chemical composition of the produced water of the stimulated gas field (g/L)

Ion concentration / mg·L ⁻¹						total mineralization
K ⁺ +Na ⁺	Ca ²⁺	Mg ²⁺	Cl ⁻	SO ₄ ²⁻	HCO ₃ ⁻	
2039	13988	9438	54652	412	808	81337

2.3 Electrochemical measurement

To investigate the effect of temperature on the performance of casing corrosion in H₂S/CO₂-saturated gas field solutions, the electrochemical measurements were conducted by a typical three-electrode system with a counter electrode made of platinum foil and saturated calomel electrode (SCE) as the reference electrode connected to the cell externally through a Luggin capillary tube positioned close to the WE to minimize the Ohmic potential drop. Polarization curves were obtained by potentiodynamic polarization technology, at a scanning rate of 1 mV/s with the scanning range of 400 mV~600 mV vs. E_{corr}. The frequency of electrochemical impedance spectroscopy (EIS) was in the range of 0.1 Hz–100 kHz with an amplitude of 5 mV for the AC stimulus signal.

3. RESULTS AND DISCUSSION

3.1 Weight-loss results

After immersion tests of 168 h, the surface corrosion scales on the specimens were subjected to a detailed surface analysis using scanning electron microscopy (SEM) and energy dispersive spectrometry (EDS), then descaled with the etching solution [18] (50 ml of 37% HCl, 5 g of hexamethylenetetramine (urotropine) and 450 ml of deionized water), dried by air and finally weighed. During the immersion tests, the change in weight from the material lost over time was used to calculate the rate of uniform corrosion using the following Eq.1 [22]:

$$v = 87600\Delta m / \rho A \Delta t \quad (1)$$

where v is the corrosion rate (mm/a), Δm is the weight loss (g), ρ is the density of steel (g/cm^3), A is the surface area (cm^2), and Δt is the corrosion time (h).

Table 3 and Figure 3 show the uniform corrosion rates of VMS110SS steel at different temperatures both in the gas phase and the liquid phase.

Table 3. Uniform corrosion rates of VMS110SS steel at different temperatures

Phase state	Uniform corrosion rate /(mm/a)				
	30°C	60°C	90°C	120°C	150°C
Vapor phase	0.256	0.491	0.838	0.543	0.485
Liquid phase	0.305	0.862	1.130	0.761	0.789

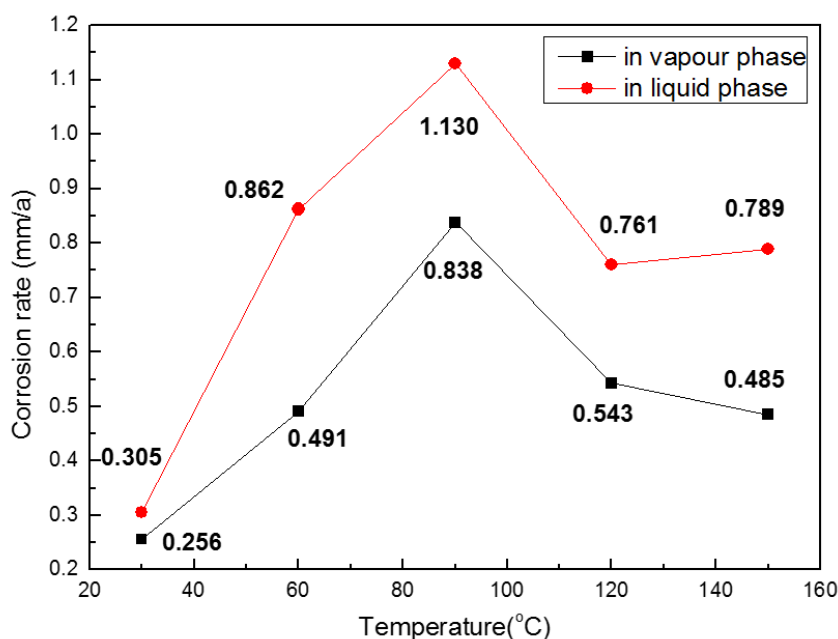


Figure 3. Corrosion rates of VM110SS steel after 168 h exposure in H₂S/CO₂ environment at normal pressure and different temperatures

It can be seen that as the temperature rises, the corrosion rates of VM110SS steel in the two-phase gas-liquid acidic environment increase exponentially, reaching the peak at 90°C, and then decrease. The total corrosion tendency appears as an inverse “v” shape, and the corrosion rates of steel are in the range of extremely severe corrosion based on the NACE RP0775-2005 standard [23]; in addition, the uniform corrosion rate of VM110SS steel in the liquid phase is far greater than that in the vapor phase, which is supported by other studies [24-26]. Therefore, in the absence of additional protection measures, VM110SS casing steels severely corrode in the H₂S/CO₂ environment, and the corrosion of the casing varies with the well depth.

The annular packer fluid containing corrosion inhibitor packages is always used to minimize any possibilities of corrosion. The comparison of corrosion rates of VM110SS steel in simulated formation water and in annular space protection solution at 90 °C is illustrated in Figure 4.

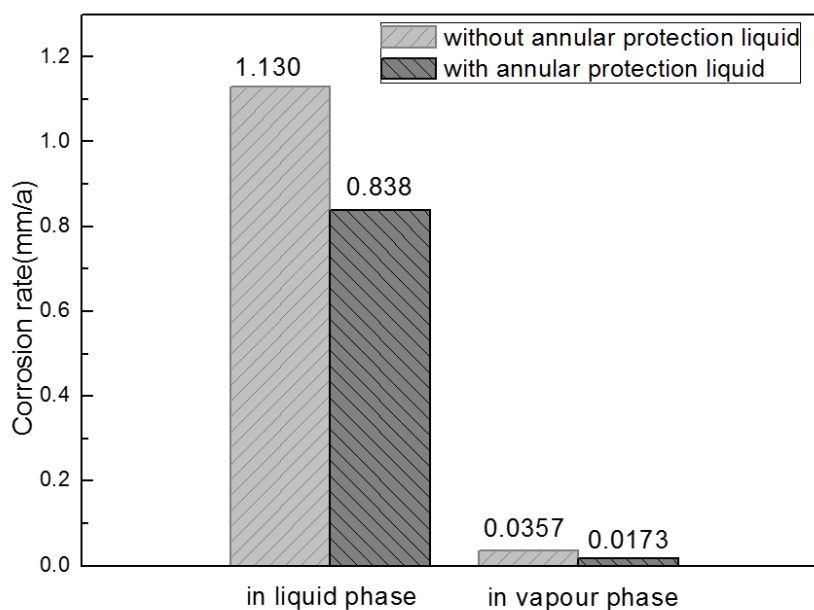


Figure 4. Corrosion rates of VM110SS steels after 168 h exposure in H₂S/CO₂ environment with/without annular space protection solution at 90 °C

As shown in Figure 4, in the aggressive H₂S/CO₂ gas field environment, the corrosion rates of VM110SS casing steel dramatically decrease with the addition of annulus protection fluid. Moreover, the corrosion rate for the vapor phase decreases from 0.0357 mm/a to 0.0173 mm/a in the presence of annular protection liquid. According to the NACE RP0775-2005 standard, it is in the range of slight corrosion. Therefore, the measures of annulus protection fluid injection and special anticorrosion coating on casing steel at 90 °C should be taken to alleviate the casing steel corrosion, which is conducive to effectively prolonging the service life of casing string.

3.2 Observation and analysis of corrosion scales

The corrosion behavior of casing steel exposed to H₂S/CO₂ gas field is greatly affected by the structural characteristics and composition of the corrosion scale. Figure 5 and Figure 6 show the microstructure of the corroded VM110SS steel coupon surface at different temperatures in both the liquid phase and vapor phase.

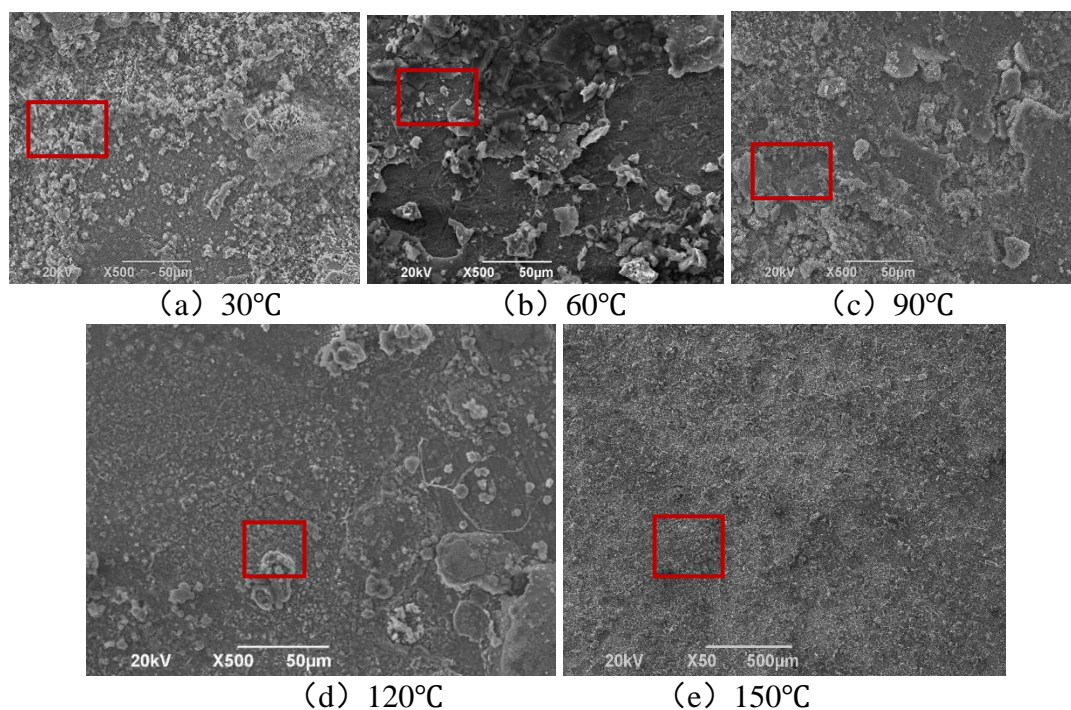


Figure 5. The microscopic morphologies of the VM110SS steel exposed in H_2S/CO_2 environment before cleaning in the liquid phase at different temperatures

It can be seen from Figure 5 that there are at least two layers of corrosion product on the metallic surface in the liquid phase. Moreover, the corrosion scale with a brittle characteristic can be observed. The thickness of the corrosion scale covering the metallic surface increases as the temperature increases from 30 °C to 90 °C. Obviously, the poor continuity and integrity of the corrosion product can also be detected (Figure 5a - c). It is noted that the loose and brittle corrosion product can be easily exfoliated from the metallic matrix surface at 90 °C (Figure 5c), which weakens its protective performance. However, compact and continuous corrosion product layers cover the specimen surface at 120 °C and 150 °C (Figure 5 d, e), and the protective layers on the metallic surface reduce the exposure of the underlying steel substrate to the aggressive fluid. The investigation is in accordance with the previous weight-loss result (shown in Table 3 and Figure 3).

Compared with the liquid H_2S/CO_2 environment, fine crystals are formed on the metal surface in the vapor phase; in addition, the distinct two-layer structure of the corrosion scale with a dense inner layer and a loose outer layer can be discovered. The corrosion scales with a flocculent structure appear on the metallic specimen surface at 30 °C (Figure 6a). Furthermore, the accumulation of corrosion products thickens, and the particle size and the gap of the corrosion products increase at 60 °C (Figure 6b). As the temperature rises to 90 °C, the corrosion scales with poor continuity can be observed, which exhibit loose and porous flocculent characteristics (Figure 6c). However, the corrosion products become compact and flat at 120 °C and 150 °C; thus, less corrosion can be observed (Figure 3). At 150°C, the polished lines of the specimen before the experiment can be found. In addition, the typical cubic characteristic of iron sulfide can also be detected on the metallic matrix surface [27].

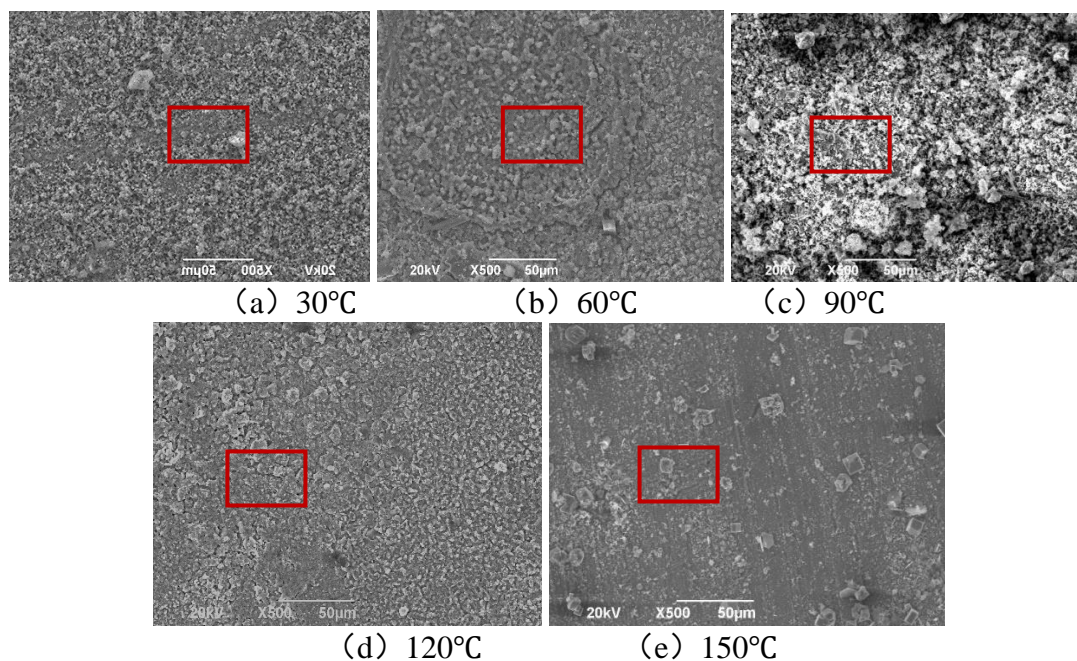


Figure 6. The microscopic morphologies of the VM110SS steel exposed in H₂S/CO₂ environment before cleaning at different temperatures in the vapor phase

Further composition analysis of the corrosion scales was conducted using EDS technology. Table 4 shows the EDS results of corrosion products on the VM110SS casing steel surface at different temperatures. The main components of corrosion products are Fe, S and O, indicating that the corrosion products may be Fe_xS_y and ferrites. The formation of ferrites can be attributed to the decomposition of FeCO₃. Iron carbonate can easily dissolve in an acid electrolyte solution due to its unsteady state [4]. In this paper, elements of Fe and S take a large proportion of the whole element weight percentage, thus verifying that H₂S dominates the corrosion process. Similar studies have reported that the sulfide corrosion layers are significantly effective in protecting the steel matrix by hindering the chemical reaction between the aggressive ions and steel surface [28-29]. The findings are further supported by results from Mei, who illustrated that the partial pressure ratio of PCO₂/PH₂S was less than 20 in a H₂S dominant system [30].

Table 4. The EDS results of VM110SS steel corrosion products at different temperatures (wt %)

Temperature, °C		O	S	Fe	Others
30	Vapor phase	6.23	31.25	61.41	1.10
	Liquid phase	7.69	35.41	55.58	1.32
60	Vapor phase	6.04	51.46	38.97	3.52
	Liquid phase	10.23	43.02	45.16	1.59
90	Vapor phase	5.64	27.61	61.64	5.02
	Liquid phase	11.68	25.67	59.57	3.08
120	Vapor phase	4.10	19.84	71.21	1.32
	Liquid phase	5.17	49.42	43.19	2.23

3.3 Corrosion electrochemical behavior

3.3.1. Polarization curve analysis

The polarization curves reflect the kinetic characteristics of the electrochemical reaction during the corrosion process. The corrosion tendency can be predicted by the corrosion potential, while corrosion current density is closely related to the corrosion rate. Figure 7 shows the potentiodynamic polarization curves of VM110SS steel at different temperatures in the H₂S/CO₂ saturated gas field solution. The R_p fitted electrochemical parameters (e.g., corrosion potential E_{corr}; corrosion current density I_{corr}; cathode Tafel slope B_c) derived from the polarization curve are displayed in Table 5.

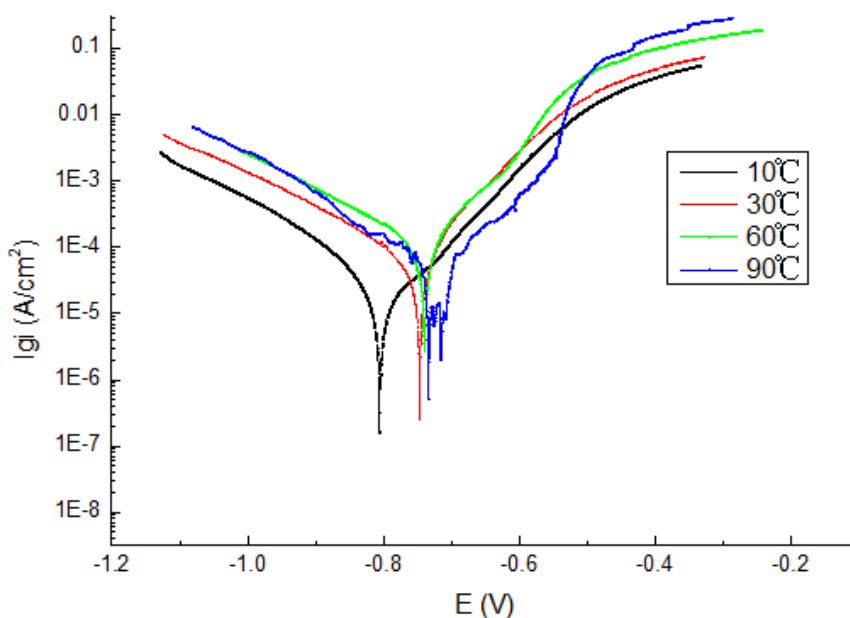


Figure 7. Polarization curves of VM110SS steel at normal pressure and different temperatures in H₂S/CO₂ saturated gas field solution

Table 5. Fitted electrochemical parameters obtained from the polarization curves

Temperatures (°C)	E(V)	B _c (mV/dec)	I _{corr} (mA/cm ²)
10	-0.806	118.810	0.0210
30	-0.747	295.570	0.0771
60	-0.741	166.440	0.173
90	-0.715	93.464	0.456

It can be seen from the polarization curves that the cathode process is greatly affected by temperature, and the corrosion reaction is mainly controlled by diffusion and activation. In addition, as the temperature rises, the corrosion potential shifts negatively and the corrosion current density of VM110SS steel increases by an order of magnitude. The observation is in good agreement with the finding of Cui, who also investigates that the influence of temperature on the cathodic process is more

noticeable than on the anodic process [31]. The corrosion current density of VM110SS steel at 90°C is 0.456 mA/cm², which increases by nearly 22 times compared to that at 10°C. The increase in temperature will lead to surface activation acceleration and promote iron matrix dissolution, thus increasing the corrosion rate. Combined with the observation of previous corrosion products, the formation corrosion scales are relatively rough and porous at 90°C, which allows corrosive ions to access and diffuse from the surface to the inner layer and even into the surface of the substrate, thus aggravating the steel corrosion.

3.3.2. EIS results

The electrochemical impedance spectroscopy (EIS) technique is used to further investigate the electrochemical corrosion behavior of VM110SS steel in the saturated H₂S/CO₂ gas field solution. Figure 8 shows the Nyquist plots of VM110SS steel at different temperatures in the H₂S/CO₂ saturated gas field solution. Moreover, the corresponding equivalent circuit model is proposed in Figure 9. In the circuit model, CPE_{dl} is the capacitance of the double electrode layer between the metal and corrosion products and CPE_f is the constant phase angle element for the surface film layer, while R_s, R_t and R_f are solution resistance, charge transfer resistance, and the film resistance of the specimen, respectively.

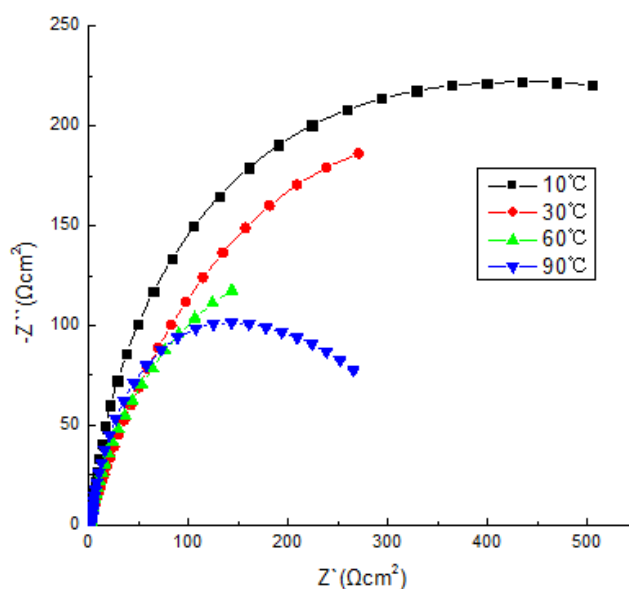


Figure 8. Nyquist plots of VM110SS steel in H₂S/CO₂ saturated gas field solution at normal pressure and different temperatures

As shown in Figure 8, the impedance spectroscopy of VM110SS steel appears as a single capacitive arc characteristic at different temperatures, and the diameter of the measured Nyquist plot decreases with the increase of temperature. According to the fitting parameters of the EIS result, both the film resistance R_f and the charge transfer resistance R_t values decrease gradually with the increase in temperature up to 90°C. According to the study by Heakal [32], the total resistance, which is inversely proportional to the corrosion rate, could be expressed by the polarization resistance R_p = R_t +

R_f . In the present study, we neglect the solution resistance R_s which is small in all cases). Obviously, with the increase of temperature, the polarization resistance R_p is significantly reduced. It is noteworthy that the film resistance R_f decreases from $221.8 \Omega \text{ cm}^2$ to $123.8 \Omega \text{ cm}^2$ with an increase of temperature, which also proves the protective performance degradation of the corrosion scale. It also has been reported in Cui's study that the temperature induced variations of the corrosion film structure is mainly responsible for the degradation of protective ability of corrosion product film [31].

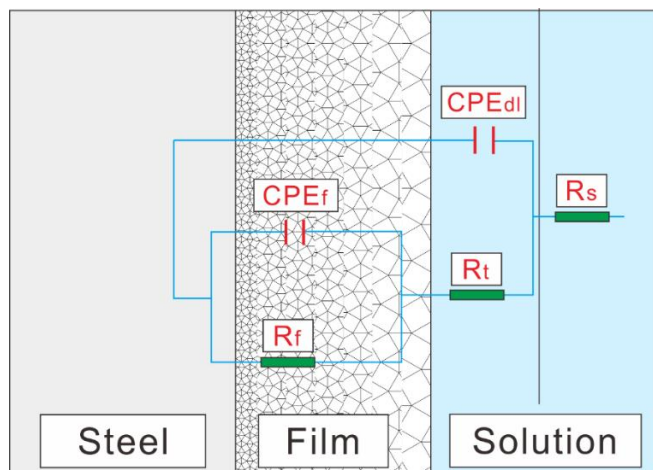


Figure 9. Equivalent circuit of VM110SS steel for simulating EIS results

Table 6. The fitted impedance parameters of VM110SS steel at different temperatures

Temperatures (°C)	R_s ($\Omega \text{ cm}^2$)	CPE_f ($F \text{ cm}^{-2}$)	CPE (P)	R_f ($\Omega \text{ cm}^2$)	$CPE(T)$ ($F/\text{cm}^{-2} \text{ Hz}^{-1}$) $CPE(P)$	CPE (P)	R_t ($\Omega \text{ cm}^2$)	R_p ($\Omega \text{ cm}^2$)
10	2.305	3.79×10^{-4}	0.93	221.8	5.67×10^{-3}	0.43	965.6	1187.4
30	2.21	6.47×10^{-4}	0.89	211.7	4.53×10^{-3}	0.72	732.6	944.3
60	1.36	3.62×10^{-4}	0.89	135.7	6.58×10^{-3}	0.58	690	825.7
90	1.02	7.55×10^{-4}	0.58	123.8	2.93×10^{-3}	0.86	466.7	590.5

The EIS investigation result in the present work is in accordance with the results obtained from the weight-loss test and morphology characterization.

3.4 Corrosion mechanism discussion

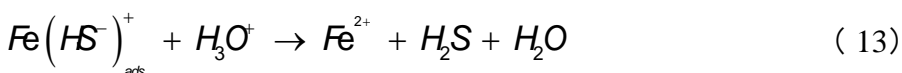
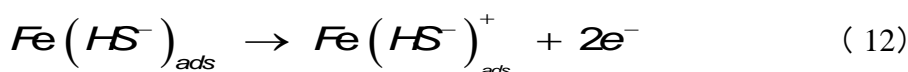
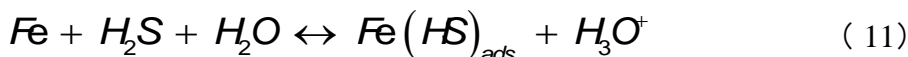
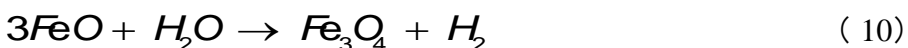
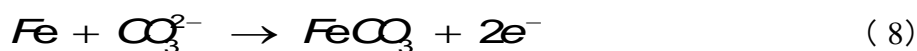
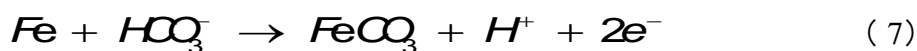
First, H_2S and CO_2 dissolve in water and form an acidic solution containing H^+ , HS^- , S^{2-} , HCO_3^- and CO_3^{2-} . The dissociation process of the acidic solution should be expressed by Eq. (2) - Eq. (6). Iron matrix is further reacted in the acid solutions by electrochemical reactions (7) – (8) and reactions (11) – (14). Once the equilibrium solubility exceeds the critical solubility, corrosion scale crystals will precipitate from the corrosive medium and deposit on the metal matrix surface. The iron sulfide is superior for precipitating on the steel surface, thus inhibiting the formation of iron carbonate.

Previous literatures indicate that the corrosion products of carbon steel are iron carbonate and iron sulfide in the wet H₂S/CO₂ environment [33-34], and the corrosion process is mainly dominated by H₂S especially when the P_{CO2}/P_{H2S} ratio is less than 20 [30]. The ratio between Fe and S, as an important characteristic parameter, can be calculated to identify the composition of the formed iron sulfide layer. Combined with the previous EDS result (Table 4), the ratio of Fe/S is more than 1 at different temperatures, indicating that the corrosion scales consist of FeS /FeS_{1-x}. In addition, a small amount of FeCO₃ generated on the steel surface will easily decompose in the reaction system or be dissolved in the acid electrolyte solution through electrochemical reactions (9) – (10). Therefore, the O element of the corrosion products may exist in the form of ferrites, which accords with Liu's investigation [4].

The dissociation process of acidic solution:



Iron matrix is further reacted in acid solutions:



At low temperatures (30°C~90°C), the iron sulfide cannot easily precipitate on the metal surface due to a large solubility constant, and the corrosion products formed on the steel surface are loose, less adherent and rich in defects. The aggressive ions diffuse through the defects, deteriorating the protective performance of the corrosion scale. The electrode reaction would be activated with the increase of temperature, promoting the steel corrosion process. When the temperature reaches 120°C, the precipitation of pyrite accumulates, forming a continuous and compact corrosion product film. The thin corrosion scale acts as a barrier to impede the access of aggressive ions, thereby depressing the metal matrix corrosion process. And the temperature induced corrosion mechanism model is proposed in Figure 10.

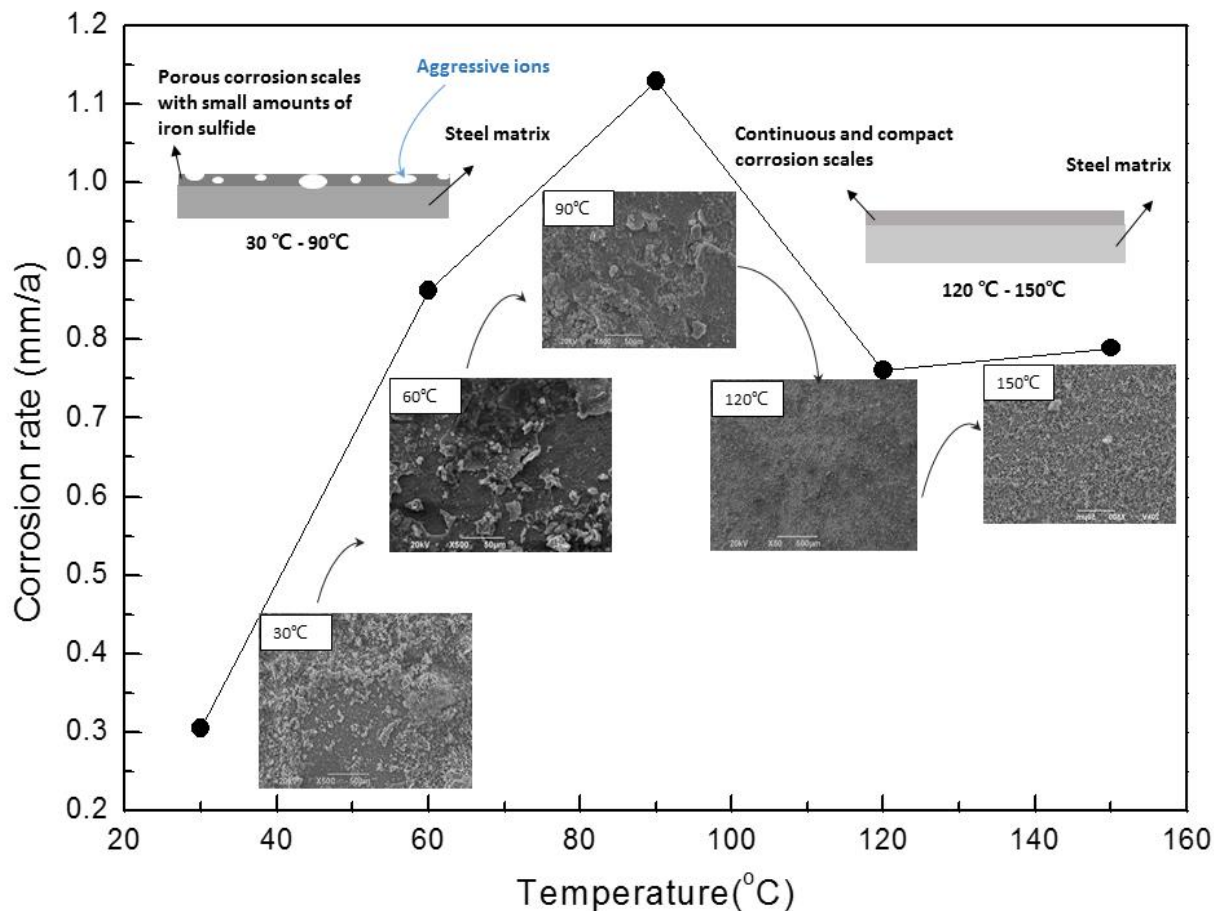


Figure 10. The temperature induced corrosion mechanism model

4. CONCLUSIONS

In this paper, the effect of temperature on the corrosion behavior of VM110SS casing steel in a CO₂/H₂S coexistent environment is investigated, and the conclusions can be drawn as follows:

(1) Corrosion attack increases in the initial stage and then decreases with the rise in temperature. The total corrosion tendency appears as an inverse “v” shape, and the corrosion rate reaches the peak at 90°C. The corrosion rates of casing steel are in the range of extremely severe corrosion based the NACE standard.

(2) The main component of the corrosion products is pyrite, and the corrosion process is dominated by H₂S. The pyrite precipitation accumulates with the increase of temperature and forms a continuous and compact corrosion product film, thus inhibiting the corrosion process.

(3) The electrochemical measurement suggests that as temperature rises, the corrosion current density gradually increases, and the polarization resistance decreases. The cathode process is greatly affected by temperature, and the corrosion reaction is mainly controlled by diffusion and activation.

(4) The annular protection fluid containing corrosion inhibitor packages dramatically decreases the corrosion rate of casing steel both in the liquid phase and in the vapor phase. Therefore, it is suggested that effective measures such as protective fluids and coating should be taken to alleviate casing steel corrosion at 90°C.

ACKNOWLEDGEMENT

The authors acknowledge the support from the National Natural Science Foundation of China (No.51774249) and National Science and Technology Major Project of China (No. 2016ZX05017-003-HZ01).

References

1. X. Guo, P. Wang, J. Liu, G. Song, H.L. Dang and T. Gao, *J. Petrol. Sci. Eng.*, 157 (2017) 999.
2. Z. Zhang, L.Y. Shao, Q.S. Zhang, C. Zhang, J. Li, D.Z. Zeng, X.K. Zhong, J.Y. Hu, D. Hou and T.H. Shi, *J. Petrol. Sci. Eng.*, 158 (2017) 729.
3. D.J. Zhu, Y.H. Lin, H.L. Zhang, Y.F. Li, D.Z. Zeng, W.Y. Liu, C. Qiang and K.H. Deng, *J. Petrol. Sci. Eng.*, 151 (2017) 311.
4. L. Liu, N. Ding, J.B. Shi, N. Xu, W.M. Guo and C.M. Lawrence Wu, *Case Studies in Eng. Fail. Anal.*, 7 (2016) 32.
5. M. Attarian, A.K. Taheri, S. Jalilvand and A. Habibi, *Eng. Fail. Anal.*, 68 (2016) 32.
6. P.C. Okonkwo, M.H. Sliem, R.A. Shakoor, A.M.A. Mohamed and M. Aboubakr, *J. Mater. Eng. Perform.*, 4 (2017) 1.
7. S. Igi, T. Sakimoto and S. Endo, *Procedia Eng.*, 10 (2011) 1451.
8. A. Afsharpour and A. Haghtalab, *Int. J. Greenh. Gas. Con.*, 58 (2017) 71.
9. H. Messabeb, F. Contamine, P. Cézac, J.P. Serin, C. Pouget and E.C. Gaucher, *J. Chem. Eng. Data*, 62 (2017) 4228.
10. Á. Rauscher and Z. Lukács, *Mater. Corros.*, 39 (2015) 280.
11. A. Robin, *British Corros. J.*, 40 (2013) 51.
12. Y. Zhou and F.A. Yan, *Int. J. Electrochem. Sci.*, 11 (2016) 3976.
13. P.P. Bai, S.Q. Zheng and C.F. Chen, *Mater. Chem. Phys.*, 150 (2015) 295.
14. J.H. Ding, L. Zhang, M.X. Lu, J. Wang, Z.B. Wen and W.H. Hao, *Appl. Surf. Sci.*, 289 (2014) 33.
15. P.P. Bai, S.Q. Zheng, H. Zhao, Y. Ding, J. Wu and C.F. Chen, *Corros. Sci.*, 87 (2014) 397.
16. Y. Zhou, P. Zhang, Y. Zuo, D. Liu and F.A. Yan, *J. Brazil Chem. Soc.*, 28 (2017) 2490.
17. J.H. Ding, L. Zhang, M.X. Lu, J.P. Xue and W. Zhong, *J. Mater. Sci.*, 48 (2013) 3708.
18. S. Li, H.G. Dong, L. Shi, P. Li and F. Ye, *Corros. Sci.*, 123 (2017) 243.
19. Y.J. Qiang, S.T. Zhang, S. Xu, L. Guo, N. Chen and I.B. Obot, *Int. J. Electrochem. Sci.*, 11 (2016) 3147.
20. Y. Qiang, S. Zhang, L. Guo, X. Zheng, B. Xiang and S. Chen, *Corros. Sci.*, 119 (2017) 68.
21. Z.F. Yin, W.Z. Zhao, Z.Q. Bai, Y.R. Feng and W.J. Zhou, *Electrochim. Acta*, 53 (2008) 3690.
22. Z. Zhang, N. Y. Zhang, Z. W. Liu and W.T. Zhao, *Mater. Corros.*, 8 (2017) 1.
23. NACE TM0177-2005, "Standard Recommended Practice for Preparation, Installation, Analysis, and Interpretation of Corrosion Coupons in Oilfield Operations".
24. Z.B. Hu, *Corros. Prot.*, 3 (2013) 269.
25. Y. Han, X.H. Zhao, F.G. Li and C.H. Lu, *J. Xi'an Technol. Univ.*, 4 (2010) 348.
26. Y.P. Fan and Y.N. Zhou, *Surf. Technol.*, 10 (2016) 180.
27. A.J. Brearley and *Meteorit, Planet. Sci.*, 38 (2003) 849.
28. B. Rutkowski, A. Gil and A.C. Filemonowicz, *Corros. Sci.*, 102 (2016) 373.
29. W. Zhao, Y. Zou, K. Matsuda and Z. Zou, *Corros. Sci.*, 102 (2016) 455.
30. P. Mei, X.Q. Qiu and J.Z. Ai, *J. Yangtze University*, 7 (2010) 1673.
31. Z.Y. Cui, L.W. Wang, H.T. Ni, W.K. Hao, C. Man, S.S. Chen, X. Wang, Z.Y. Liu and X.G. Li, *Corros. Sci.*, 118 (2017) 31.
32. F. Heakal, A. Fekry and A. Ghoneim, *Corros. Sci.*, 50 (2017) 1618.
33. N.Y. Zhang, D.Z. Zeng, G.Q. Xiao, J.F. Shang, Y.Z. Liu, D.C Long, Q.Y. He and A. Singh, *J. Nat. Gas Sci. Eng.*, 30 (2016) 444.

34. S.Z Tan, G.Q. X, A. Singh, J. F. Shang, D.C Long, N.Y. Zhang, D.Z Zeng and E.E. Ebenso, *Int. J. Electrochem. Sci.*, 12 (2017) 5742.

© 2018 The Authors. Published by ESG (www.electrochemsci.org). This article is an open access article distributed under the terms and conditions of the Creative Commons Attribution license (<http://creativecommons.org/licenses/by/4.0/>).